Supplemental Material for "Superconducting triangular islands as a platform for manipulating Majorana zero modes"

Aidan Winblad[1] and Hua Chen[1,2]

[1] *Department of Physics, Colorado State University, Fort Collins, CO 80523, USA*
[2] *School of Advanced Materials Discovery, Colorado State University, Fort Collins, CO 80523, USA*

I. MANY-BODY BERRY PHASE CALCULATION FOR THE 3-SITE KITAEV TRIANGLE

In this section we provide details for calculating the many-body Berry phase for braiding two MZM in the Kitaev triangle, as shown in Fig. 2 in the main text. To start we use the Hamiltonian Eq. (1) in the main text,

$$\mathcal{H} = \sum_{\langle jl \rangle} (-t e^{i\phi_{jl}} c_j^\dagger c_l + \Delta e^{i\theta_{jl}} c_j c_l + \text{h.c.}) - \sum_j \mu c_j^\dagger c_j, \tag{1}$$

We then write the creation and annihilation operators in the following Fock space basis for three spinless fermions

$$\begin{aligned}(|0\rangle, |1\rangle, \ldots, |7\rangle) \equiv & \{|n_1, n_2, n_3\rangle\} \\ = & \big(|0,0,0\rangle, \\ & |1,0,0\rangle, |0,1,0\rangle, |0,0,1\rangle, \\ & |0,1,1\rangle, |1,0,1\rangle, |1,1,0\rangle, \\ & |1,1,1\rangle\big)\end{aligned}$$

The creation(annihilation) operators in this space are defined as

$$\begin{aligned} c_j^\dagger |n_1, \ldots, n_j, \ldots\rangle &= \sqrt{n_j+1}(-1)^{s_j} |n_1, \ldots, n_j+1, \ldots\rangle, \\ c_j |n_1, \ldots, n_j, \ldots\rangle &= \sqrt{n_j}(-1)^{s_j} |n_1, \ldots, n_j-1, \ldots\rangle, \end{aligned} \tag{2}$$

where

$$s_j = \begin{cases} \sum_{l=1}^{j-1} n_l & j > 1 \\ 0 & j = 1 \end{cases} \tag{3}$$

For the initial configuration corresponding to $\boldsymbol{\phi}_1$ in Eq. (6) of the main text, diagonalizing the 8×8 BdG Hamiltonian in the above basis leads to two degenerate ground states that can be distinguished by the occupation number of the following fermion operator constructed from the two MZM at the two bottom vertices

$$c_M \equiv \frac{1}{2}(a_1 + i b_2), \; n_M \equiv c_M^\dagger c_M \tag{4}$$

The two degenerate ground states for the initial configuration, denoted as $|0\rangle_i$ and $|1\rangle_i$, therefore satisfy

$$\begin{aligned} n_M |0\rangle_i &= 0, \\ n_M |1\rangle_i &= |1\rangle_i \end{aligned} \tag{5}$$

In practice, we first construct the operator R_{gs} as a 8×2 matrix by combining the two column eigenvectors of the two lowest-energy eigenstates of the initial BdG Hamiltonian:

$$R_{\text{gs}} \equiv (\psi_i, \psi_i') \tag{6}$$

and then diagonalize the projected n_M operator:

$$U_n^\dagger (R_{\text{gs}}^\dagger n_M R_{\text{gs}}) U_n \equiv R_i^\dagger n_M R_i = \begin{pmatrix} 0 & \\ & 1 \end{pmatrix} \tag{7}$$

To carry out the Berry phase calculation we next need to adiabatically "rotate" the vector potential field by following the linearly interpolated closed parameter path described in the main text, which is discretized into $N+1$ segments. At any given point labeled by j along the path, we diagonalize the corresponding Hamiltonian and construct the projection operator P_j using the two lowest-energy eigenvectors ψ_j, ψ'_j:

$$P_j \equiv \psi_j \otimes \psi_j^\dagger + \psi'_j \otimes \psi_j'^\dagger \tag{8}$$

where $\otimes$ means tensor product. The 2×2 Berry phase matrix $M_{f\leftarrow i}$ for the given parameter path is then obtained as

$$M_{f\leftarrow i} = \lim_{N\to\infty} R_f^\dagger P_N P_{N-1} \dots P_1 R_i \tag{9}$$

where $R_f = R_i$ since the path is closed.

By using a large enough N we found the converged $M_{f\leftarrow i}$ matrix has only diagonal elements being nonzero, meaning the braiding only changes each ground state by a scalar phase factor. Their values are $(M_{f\leftarrow i})_{00} = e^{i0.118\pi}$ and $(M_{f\leftarrow i})_{11} = e^{-i0.382\pi} = e^{i(0.118-0.5)\pi}$.

We end this section by noting that the parameter path considered for the 3-site Kitaev triangle above is not equivalent to rotating a staggered vector potential but to separately manipulating the Peierls phases along the three edges. We have also done calculations for the latter case and found the two lowest-energy states fail to be degenerate everywhere along the parameter path, leading to non-standard Berry phase values.

II. MAJORANA CORNER MODES FOR FINITE-WIDTH TRIANGLES

A model that is closer to a realistic hollow triangular island is the finite-width triangular chain or ribbon. An example, illustrated in Figure 1 (c), has its edge length $L = 50$ and width $W = 3$. The phase diagram Fig. 1 (a) is created in a similar way as that in Fig. 3 (a) of the main text, assuming a constant vector potential $\mathbf{A} = A\hat{\mathbf{y}}$ and infinitely long $W = 3$ ribbons. The spectral flow for the actual triangle with $\mu = 1.6$ in Fig. 1 (b) show MZM in the correct regions expected from the phase diagram. Fig. 1 (c) plots the MZM wavefunction for $A = 2.7409$ and $\mu = 1.6$ that are indeed well localized at the bottom corners.

We next rotate the uniform vector potential to examine how the MZM move on a hollow triangle. Figure 2 shows the spectral flow and eigenfunctions as we rotate $\varphi = 0$ to $\varphi = \pi$ counterclockwisely. The two MZM cycle through the three vertices as φ increases from 0 to $\pi/3$ in a similar manner as that in Fig. 4 of the main text.

III. BRAIDING MZM IN A SMALL NETWORK OF TRIANGLES

It is now pertinent to see if we can use the previous results to interchange two MFs that are not paired together. We initialize three triangular chains adjavent to each other, connecting their bottom corners together. The left and right triangles initialize a constant vector potential with $\varphi = 0$, while the middle island will initialize with $\varphi = \frac{\pi}{6}$. Slowly rotating the middle triangle chains vector potential to $\varphi = \frac{\pi}{3}$ we see the the middle MFs swap which MF pair they are connected to.

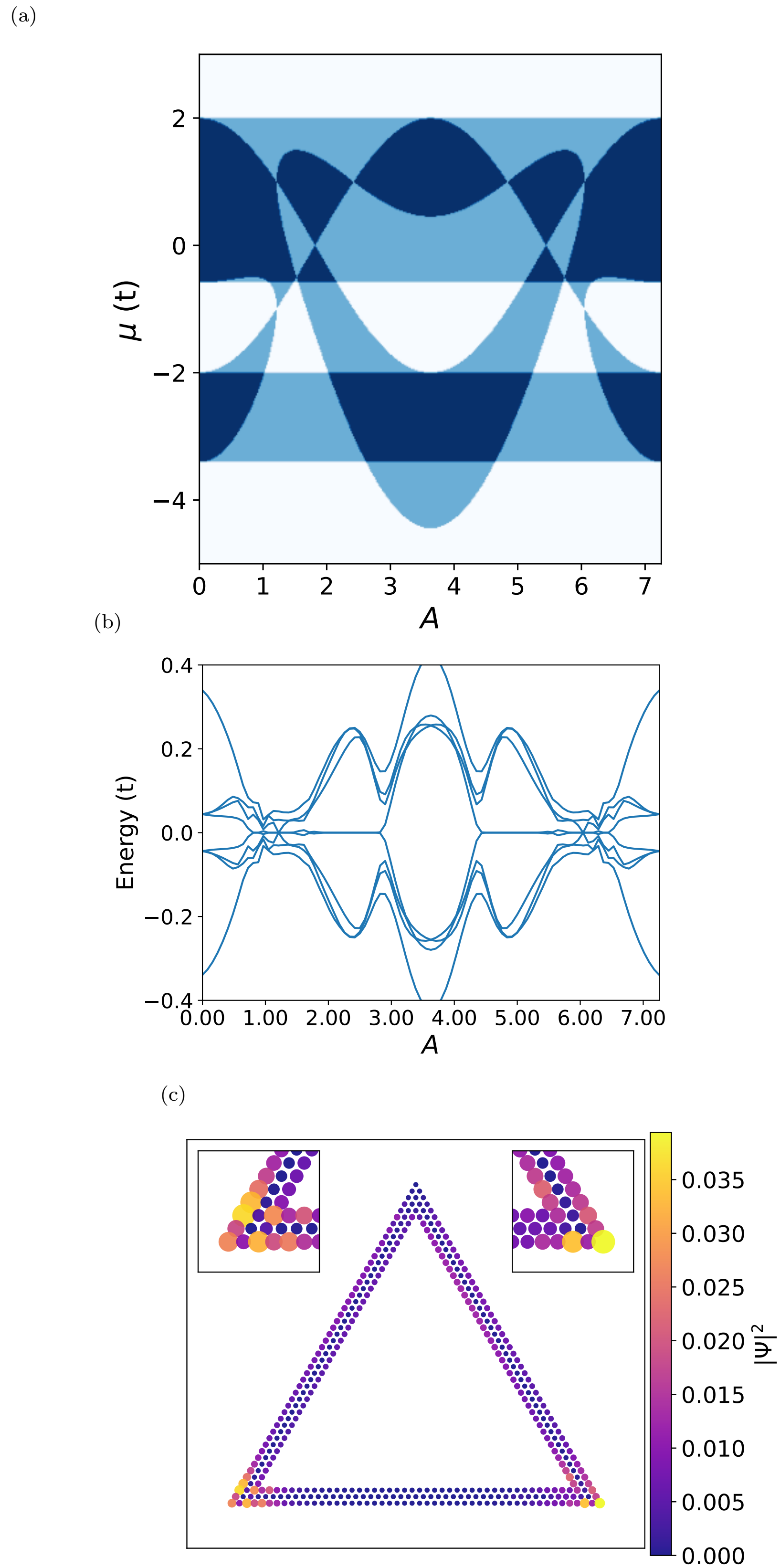

FIG. 1. (a) Topological phase diagram for a $W = 3$ hollow triangle obtained by overlapping the $\mathcal{M}(A, \mu)$ plots of 1D chains with $\mathbf{A} = A\hat{\mathbf{y}}$ and $\mathbf{A} = A(\frac{\sqrt{3}}{2}\hat{\mathbf{x}} + \frac{1}{2}\hat{\mathbf{y}})$. Color scheme: white—$\mathcal{M} = 1$, dark blue—$\mathcal{M} = -1$, light blue—$\mathcal{M} = 0$ (b) Near-gap BdG eigen-energies vs A for a finite triangle with edge length $L = 50$, $W = 3$, and $\mu = 1.6$. (c) BdG eigenfunction $|\Psi|^2$ summed over the two zero modes at $A = 2.4709$.

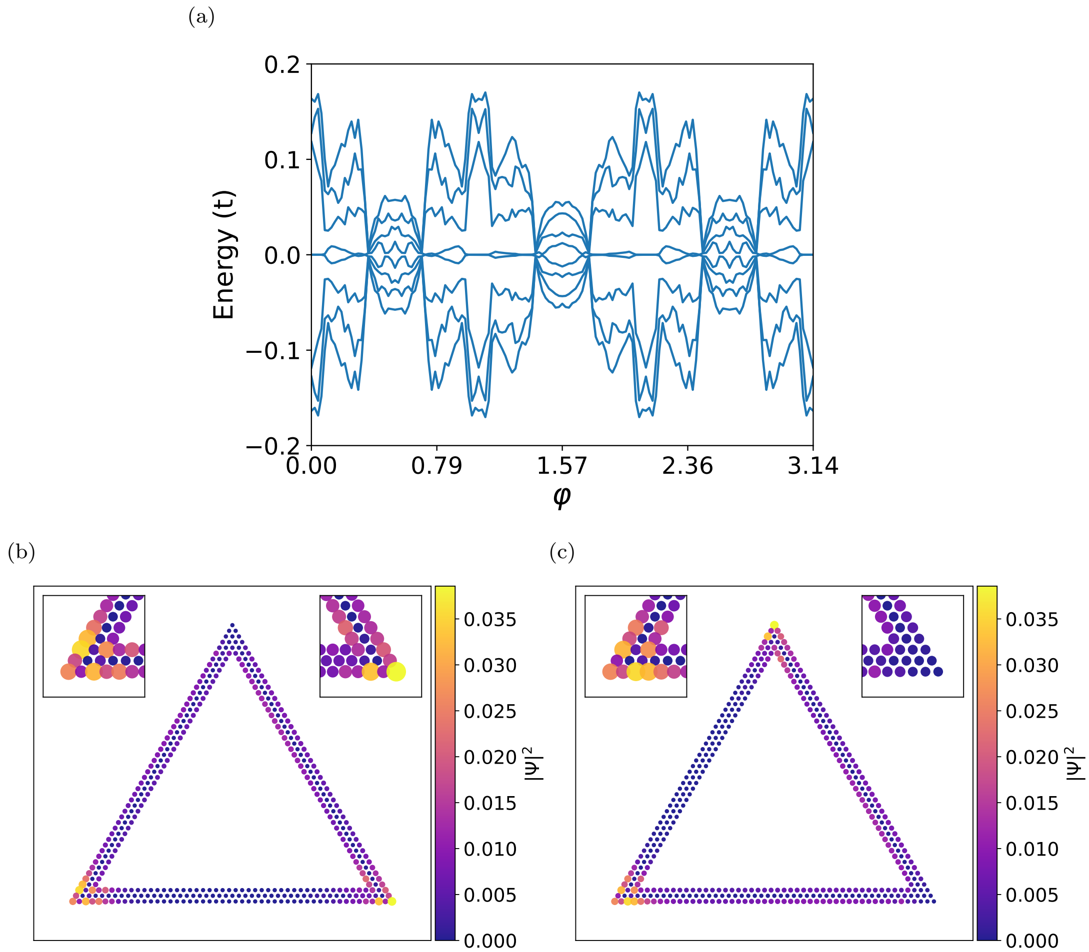

FIG. 2. (a) Spectral flow of a hollow triangle with $W = 3$, $L = 50$, $\mu = 1.6$, and $A = 2.75$ with increasing rotation angle φ, defined through $\mathbf{A} = A(-\sin\varphi\hat{\mathbf{x}} + \cos\varphi\hat{\mathbf{y}})$. (b-c) BdG eigenfunction $|\Psi|^2$ summed over the two zero modes at $\varphi = 0$ and $\frac{\pi}{3}$, respectively.

(a)

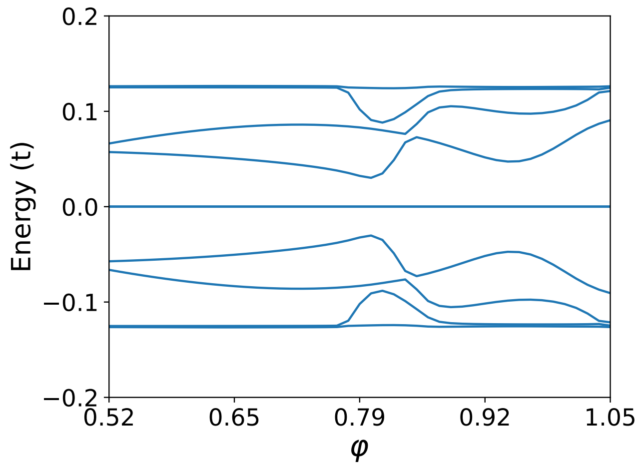

(b)

(c)

(d)

(e)

(f)

(g)

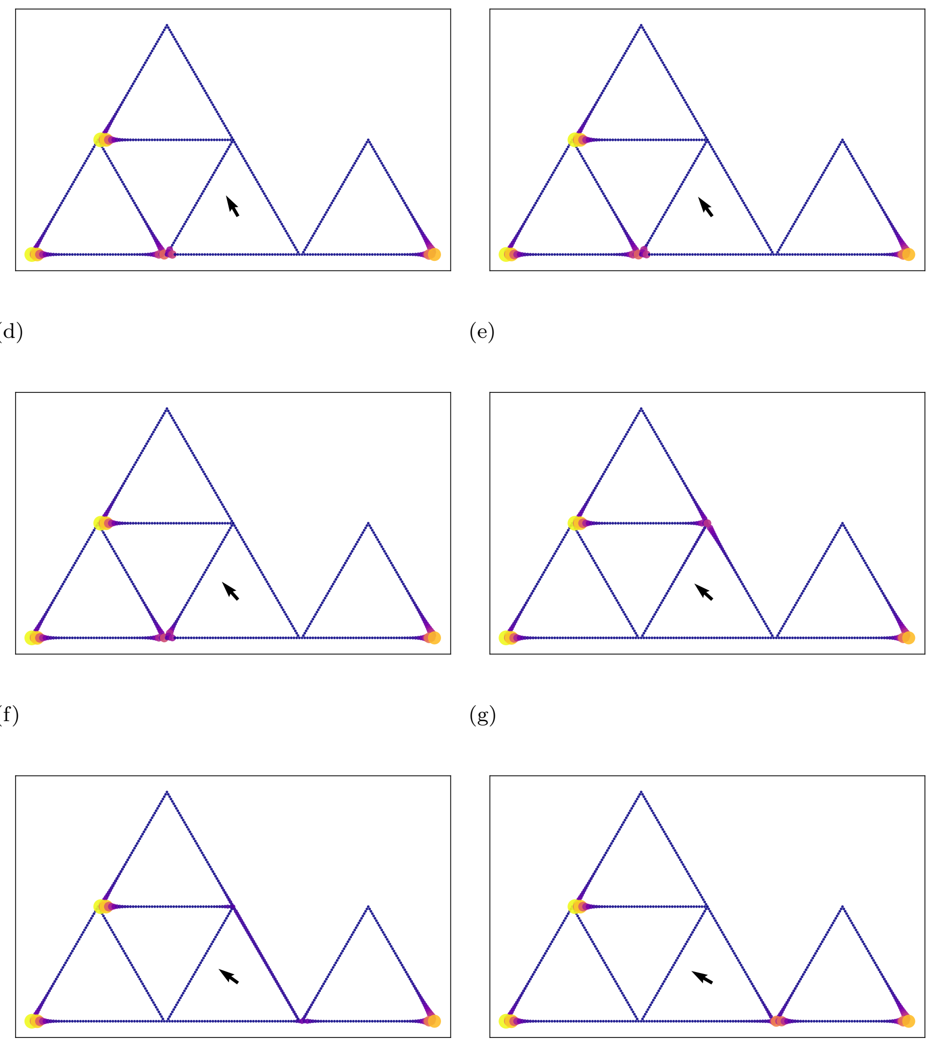

FIG. 3. (a) Spectral flow of three triangular chains connected at their bottom certices in a row with $W = 1$, $L = 50$, and $\mu = 1.6$. Each triangle has a vector potential field applied as $\mathbf{A} = A(\sin\varphi\hat{\mathbf{x}} + \cos\varphi\hat{\mathbf{y}})$, with $A = 2.6$. The left and right trianlges have $\varphi = 0$, while the middle triangle rotates $\varphi = \dfrac{\pi}{6}$ to $\varphi = \dfrac{\pi}{3}$. (b)-(f) BdG eigenfunction $|\Psi|^2$ summed over the four zero modes over the rotation of the middle triangles φ.